Drilled Shaft Grouting Effectiveness in Mekong Delta

Hai M.N.[1], Anand J.P.[2], Long D.P.[3] and Trung T.N.[4]
[1]*Department of Geotechnical Engineering, Geotech Engineering and Testing, Houston, USA*
[2]*Department of Civil Engineering, University of Texas at Arlington, Arlington, USA*
[3]*Vietnam Society for Soil Mechanics and Geotechnical Engineering, Hanoi, Vietnam*
[4]*Department of Civil Engineering, HoChiMinh University of Technology, HCM, Vietnam*
[1]*E-mail*: haitdmu@gmail.com
[2]*E-mail*: anand@uta.edu
[3]*E-mail*: long.phung@gmail.com
[4]*E-mail*: nguyenthanhtrung.ce@gmail.com

ABSTRACT: In recent years, the post shaft-grouting technique has been used prevailingly for improving the drilled shaft bearing capacity of the high-rise building foundation projects in Mekong River basin of Vietnam. However, the effectiveness of the post shaft-grouting works for the drilled shafts is rarely obtained as expected. This paper will present results of bidirectional tests on the non-grouted and grouted shafts of the Lancaster Lincoln high-rise building project in Ho Chi Minh City, Vietnam, performed in 2016. The test shafts had diameter of 1.5 m and were constructed to 85 m depth below ground surface. The shaft grouting was performed along about 49 m above the drilled shaft toe level. The bidirectional load test results and the analysis shows that the unit shaft resistances of the sand and clay layers were increased about 150 and 300 percent after grouting, respectively.

KEYWORDS: Shaft grouting, Bidirectional load test, Movements, Strain, Shaft resistance, load distribution, Elastic Shortening

1. INTRODUCTION

The geology of Mekong River basin in Vietnam consists of the surficial soft clay with thickness of hundred meters. Deep drilled shafts are usually needed in order to support the high-rise building foundations. For the drilled shaft foundation design for the high-rise buildings in this area, the toe resistances are normally ignored by virtue of cleaning difficulty of the soft soils accumulated at the bottom of hole during drilling. Moreover, negative skin friction within the surficial soft clay soil will introduce the additional settlement, downdrag, for the drilled shaft foundation, which requires the shafts to be significantly lengthened to meet the required limits for settlements.

In recent years, the post shaft-grouting techniques have been developed to improve the bearing capacity of the drilled shafts and enable reducing the length of the drilled shafts, thus saving construction costs. Although, much field research on the shaft resistance improvement of the drilled shafts have been performed (Bolognese and Amoretto, 1973; Bruce, 1986; Nguyen and Fellenius, 2015; Nguyen et al., 2016), observation on the effectiveness of the post shaft-grouting works are limited. Successful level of each project depends on many factors such as the characteristics of soil, the grouting pressures, the grouting mix ratio, the arrangement of grouting tubes, the perforation along the installed grouting tubes, etc. The authors have a strong belief that the presented case history of a post shaft-grouting foundation project will be valuable to geotechnical engineers working on such projects.

This paper presents the test results of two drilled shafts constructed for the 40-storey Lancaster Lincoln Building in Ho Chi Minh City, Vietnam. One of the two drilled shafts were grouted to improve the shaft resistance. The soil stratigraphy at the project site consisted of soft to firm clay to 36-m depth deposited on medium dense to dense silty sand to 44-m depth, followed by firm to stiff clay to depth of 65 m, medium dense to dense silty sand to depth of 75 m and stiff clay to depth of 79 m, and underlain by silty sand. The constructed shafts had diameter of 1.5 m and length of 85.0 m. The drilled shafts were attached with the strain gages at the different depths along the drilled shaft lengths. One of the two test piles was grouted along about 49 m shaft above the toe to improve the shaft resistance. Bidirectional static loading tests were performed on the drilled shafts to evaluate effectiveness of the post-grouting.

2. SOIL CONDITIONS

The soil conditions at the project site were explored by five geotechnical borings to depths from 60 through 100 m below the existing grades. The locations of borings and the tested drilled shaft are shown on Figure 1. As can be seen from Figure 1, the location of boring BH-3 is closest to the tested drilled shafts. Therefore, the soil properties obtained from boring BH-3 will be used to evaluate the shaft resistances of the tested drilled shafts.

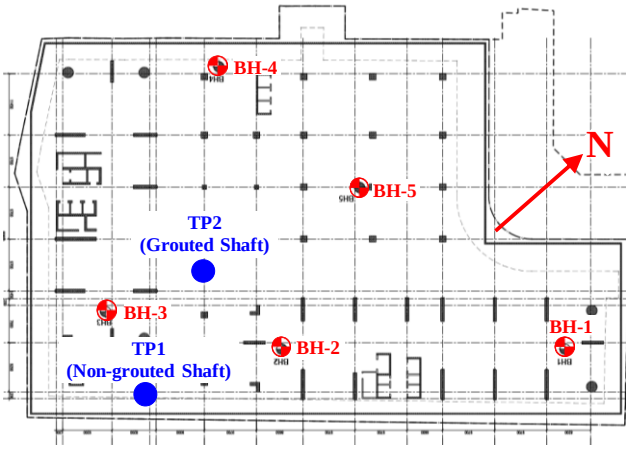

Figure 1 Layout of borings and the tested drilled shafts, TP1 and TP2

The soil stratigraphy of the boring BH-3 consisted of soft to firm clay to 36-m depth deposited on medium dense to dense silty sand to 45.5 m depth, followed by firm to stiff clay to depth of 55.5 m, medium dense to dense silty sand to depth of 73.5 m and stiff clay to depth of 79.5 m, and underlain by silty sand. Figure 2 shows the distribution of water content, consistency limits, grain-size distribution, and SPT N-indices determined from the borehole records. The average saturated density and water content of the clay were about 1,800 kg/m3 and 40%, respectively. The average density of the sand was about 2,100 kg/m^3. The groundwater table was located at a depth of about 1.0 m below the ground surface.

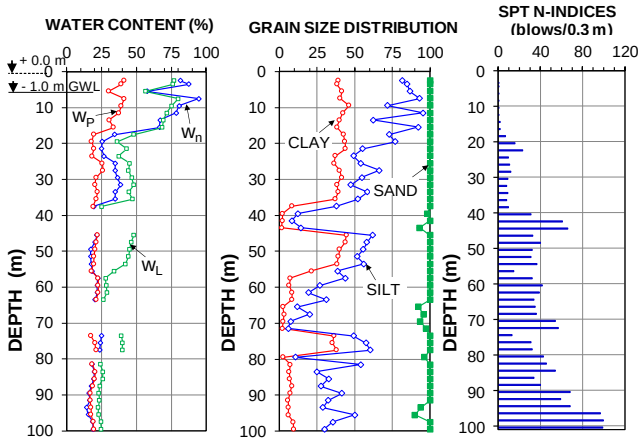

Figure 2 Water content, soil type proportions, and N-indices

3. CONSTRUCTION OF DRILLED SHAFTS

Two drilled shafts were constructed using a bucket with bentonite slurry and a clean-out bucket for cleaning the bottom of the drilled holes. The nominal diameter of both drilled shafts was about 1,500 mm. The shafts, TP1 and TP2 were drilled on August 09 and 11, 2016, respectively. The construction of the shafts was started by inserting the casings of outer diameter about 1,540 mm through the subsurface soft clay soil layer into a depth of 18 m and then a drilling bucket was used to drill into a depth of about 85 m below ground surface. Before lowering the reinforcing cages and placing concrete, a clean-out bucket used to clean the soft soils accumulated at the bottom of drilled holes during drilling. Bentonite slurry was used to support and maintain the hole. The bentonite slurry properties monitored after completed drilling for both shafts indicated a density of 1,020 kg/m3, 36-s Marsh viscosity, pH of 9, and final maximum sand content of 1.0%.

After cleaning the bottom of the drilled holes, the reinforcing cages with the attached bidirectional cell assemblies were inserted into the drilled holes. Concrete was then placed by tremie to the bottom of the drilled holes through a 250 mm O.D until the top of concrete reached the ground surface. A reinforcing cage made up of thirty-two 32 mm bars was inserted in each shaft, resulting in a steel reinforcement area of 260 cm^2 and a reinforcement ratio of 1.5 % of the 1.77 m^2 total nominal pile cross section. The compressive strengths of the concrete cylinder at the pile test time (about 28 days after casting) were about 64 and 62 MPa for the drilled shafts TP1 and TP2, respectively.

Figure 3 shows the locations of the vibrating wire strain-gages attached to the reinforcing cages (five levels below and ten levels above the bidirectional cell level) for each test shaft. Each gage level (GL) contained two diametrically opposed pairs. Additionally, Figure 2 also indicates the cut-off level of the construction piles at 10 m depth below the ground surface, i.e., depth of the future lowest basement level.

To arrange and facilitate the drilled shaft grouting TP2, five 60 mm diameter pipes were attached around the perimeter of the reinforcing cage spaced at 72-degree angle throughout the 49-m shaft length above the drilled shaft toe. The concrete cover outside the grout pipe was 15 mm thick. Over the lower 49 m length of shaft TP2, the pipes were perforated for grout release and covered by a tight-fitting rubber sleeve. Grouting was carried out by means of inserting a "Tubes-à-Manchette" grouting tube with packers ("manchettes") that allow the grouting to be directed to a specific length (1.0 m) of the grout pipe at a time.

Two days after placing the concrete, the shaft TP2 was grouted. Before shaft grouting was conducted, the shaft concrete cover was cracked by pumping high pressure water through the grout tubes. The fact that the cracking of the concrete cover had been accomplished was signaled by a sudden drop of the water pressure occurring at 3.0 MPa pump pressure. The water was then turned off and cement grout was pumped down through the grout pipe expelling the water and forcing the grout out into the soil immediately outside the shaft. The maximum grout pressure measured at the grout pump was about 4.0 MPa. A water-cement ratio of 0.55 was used for all grouting mixtures. The total grout volumes for pile were about 8.6 m^3. Assumed to spread evenly along the pile perimeter, these volumes indicated an about 37 mm thick grout zone. Theoretically, adding this grout zone evenly to the shaft circumference and area means a 2.5% increase of circumference and a 5.0% increase of shaft cross section area.

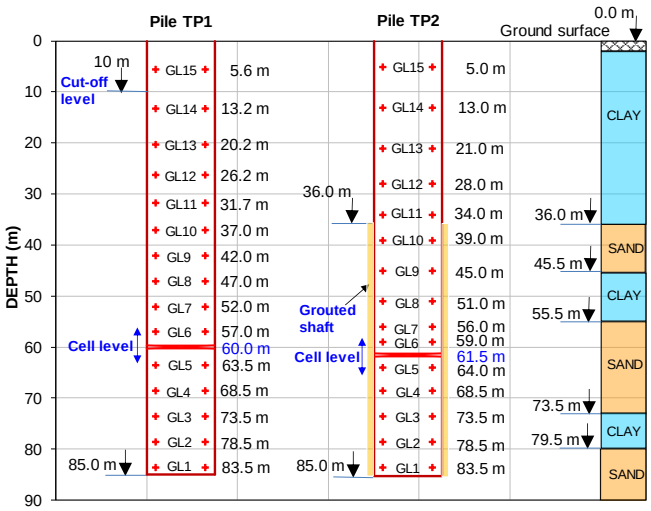

Figure 3 Details of shaft grouting and instrumentation

4. LOAD TEST PROGRAMME AND MEASUREMENTS

4.1 Loading Schedule

The bidirectional loading tests for the drilled shafts were carried out in two loading cycles for the non-grouted shaft TP1 and one loading cycle for the grouted shaft TP2 (Loadtest Pte. Ltd., 2016). Figure 4 shows the load vs. time schedule. The Cycle 1 loading for both drilled shafts was performed by means of a first load-increment of 2.55 and 3.06 MN, respectively, followed by nineteen and thirty increments ranging from about 0.81 through 1.61 MN to a maximum load of 21.64 and 42.46 MN, respectively. Each of the first nineteen and twenty-three load increments of Cycle 1 was held constant for ten minutes and the 20th and 24th load increment was held for thirty and sixty minutes, respectively. For the drilled shaft TP2, seven additional load increments of 1.21 through 1.61 MN held for 5 minutes were added after the one-hour load-holding of Cycle 1 to a maximum load of 42.46 MN before unloading in eight steps. The test shaft TP1 was unloaded in four steps. Each of the first three and seven unloading steps was held for 10 minutes. The last fourth and eighth unloading step was held for 30 minutes.

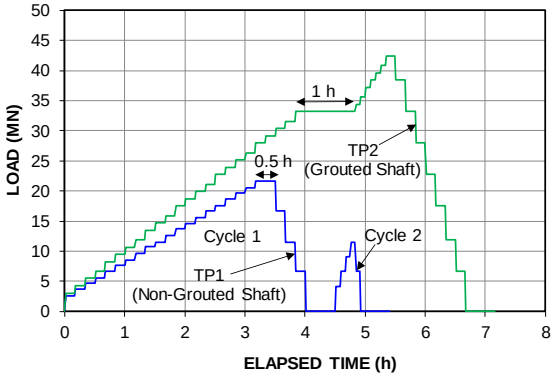

Figure 4 Loading schedule for the non-grouted and grouted shafts

In Cycle 2, only shaft TP1 was first reloaded to the 11.55-MN load in four increments and unloaded in two steps. Each of four load increments and the first unloading was held for 5 minutes. The last unloading step was held for 30 minutes. It should be noted that the uneven magnitude of load increments and varying load-holding durations were additional sources of disturbance for the strain-gage measurements.

4.2 Load-Movement Measurement

Figure 5 shows the measured upward and downward load-movement curves of the bidirectional tests for the drilled shafts TP1 and TP2. Loads measured are not adjusted for pile weight and water pressure at the cell level. For the maximum test loads of 21.64 and 42.46 MN, the maximum downward and upward movements measured were about 10.6 through 16.8 mm and 33.8 through 23.3 mm for the shaft TP1 and TP2, respectively. The maximum head and toe movements were about 7.2 through 3.4 mm and 8.5 through 22.1 mm, respectively.

As can be seen from in Figure 5, the load-movement curves are strain-hardening, and this reflects that the ultimate bearing capacities of the tested shaft were not reached. It should be noted that the remarkable movements recorded at the last load increment of the grouted shaft TP2 (for the last load increment from 40.86 to 42.46 MN, the upward and downward movements recorded were about 3.6 and 6.7 mm, respectively). For these movement values, it is likely that the shaft shear resistances above the cell level was mobilized fully (Fellenius and Nguyen, 2015); however, the toe resistance of the drilled shaft was not mobilized fully due to the toe of the drilled shaft located in the dense sand as shown in Figure 1 and 2 (Fellenius, 2018). The significant movement of the toe of the drilled-shaft recorded in this case implies that the soil below the toe was soft.

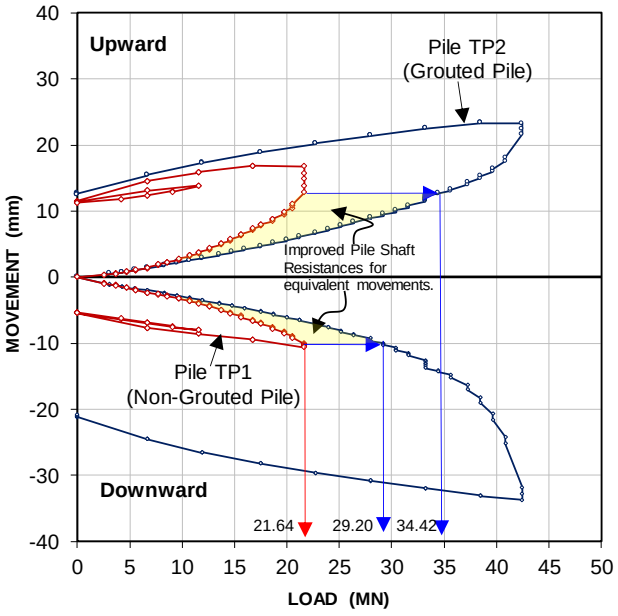

Figure 5 Measured load-movement curves of shafts TP1 and TP2

Another imortant information obtained from the load-movement curves of two tested shafts is the effectiveness of the shaft-grouting works. To preliminarily evaluate the effectiveness of the grouted shaft TP2, it is necessary to select a target movement for use as reference. From load-moevement curves in Figure 5, the most suitable target values for TP1 are the maximum measured upward and downward movements, excluding the movements measured in the last load-holding time. The maximum movements of the grouted test shaft TP2, the corresponding test loads were about 29.2 and 34.4 MN, respectively, which values are about 1.35 and 1.59 times greater than the maximum test load of the non-grouted shaft TP1. Assuming that the toe resistances are similar, the average shaft resistance of TP2 is about 1.5 times greater than the non-grouted shaft resistance of TP1.

It should be noted that the shaft segment below the cell level for TP2 is about 1.5 m shorter than for TP1. If both the shaft segments below the cell level had been the same, the effectiveness of the grouted shaft resistance would have been greater than 1.5.

4.3 Strain Gage Measurement

The strain gage installation, measurement and analysis of the drilled shafts are relatively complex. The strain gage pairs on each cross-section area should be placed diametrically opposed and parallel with the axial center line of the drilled shafts. At the different levels, the strain gages should be placed on the same vertical line. Even if the above requirements of the strain gage installation are satisfied, the strains measured on each cross-section area are also significantly different. Therefore, to select a reasonable strain value on each cross-section area for analysis, the average calculation of all the measured strain gages, or a measured strain gage pair, or one measured strain gage depends on many factors, such as the tested load, the residual load, the adjacent strain gages, soil conditions, etc. The problems of the strain gage installation and measurements were reported by many researchers, such as Fellenius (1989, 2001, 2002, 2018), Nguyen, et al (2016).

Figures 6 and 7 present the measured load-strain curves of the drilled shafts TP1 and TP2, respectively. The upper and lower diagrams of Figures 6 display the load-strain curves of shaft TP1 measured from the train gage levels below and above the cell levels, respectively. It should be noted that only the strain measurements of the eleven gage levels are presented in Figures 6 and 7 because these gage levels are useful for evaluating the effectiveness of the drilled shaft resistances. For these different gage levels, GL12 through GL15, the strains induced by the test loads are not significant. In addition, the strain measurements of the gage levels below and above the cell levels are separated to consider the stiffness of the drilled shafts. The authors believe that it is reasonable to consider two separated shaft stiffness for the bidirectional loading tests because (1) the shaft construction below the cell level is normally more difficult than above the cell level due to presence of the installed cell equipment. This will result in the inhomogeneous material quality between the shaft below and above the cell level, (2) the shaft segment below the cell level has to mobilize both the shaft shear and toe resistance for an imposed test load, while the shaft segment above the cell level only mobilizes the shaft shear resistance. Therefore, the strains induced by an imposed test load for each shaft segment is different. Details of this subject will be examined in the following sections.

As can be seen from the upper diagrams of Figure 6 (the gage levels below the cell level), the measured strains of the gage level GL4 are anomalous. Therefore, the strain records at this gage level will be ignored in analysis of the shaft resistance. The gage level GL5 was installed near the cell level as shown on Figure 3 and its load-strain curve is relatively linear, which is suitable for evaluating the drilled shaft stiffness below the cell level due to less affected by the resistance of soil. The slope of this load-strain curve is known as the shaft stiffness, AE, and estimated is about 62 GN. The lower diagrams of Figure 6 (the gage levels above the cell level) show that the strains measured at the gage levels GL8 and GL9 are greater than GL8 and GL9, respectively. It is clear that this is not reasonable. The shaft stiffness estimated the gage levels GL6 and GL7 is about 62 GN, which is equivalent to the shaft stiffness below the cell level determined from the gage level GL5; while, the shaft stiffness estimated from the gage levels GL8 and GL9 is about 42 GN. In this case, only one of the two gage level pairs measured either GL6 through GL7 or GL8 through GL9 are reliable for analysis. To know which gage level pair are reasonable and reliable for analysis, it is necessary to consider the same-depth strain measurements of the grouted shaft TP2.

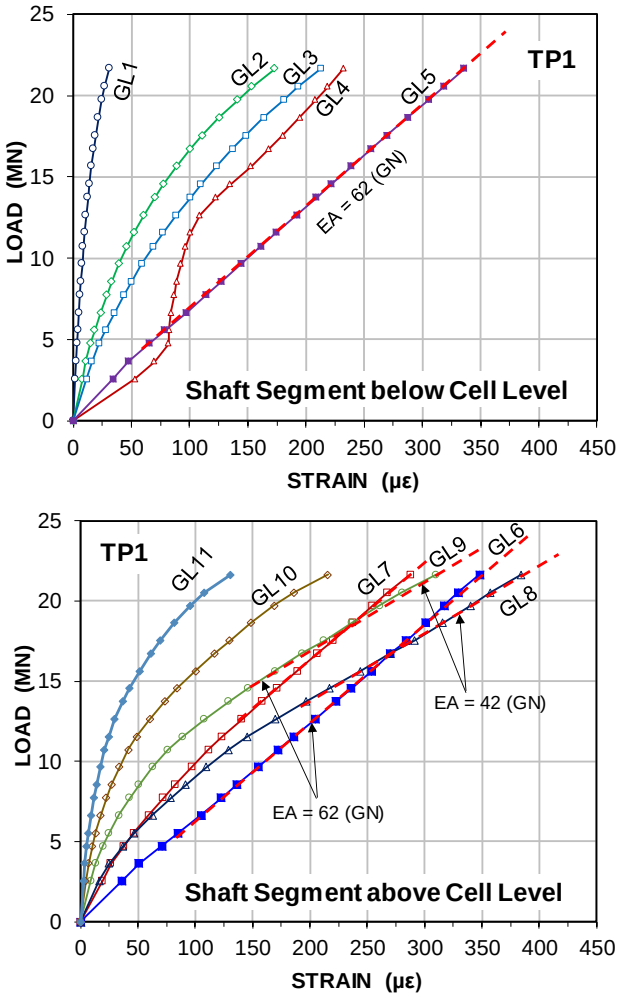

Figure 6 Load versus strain curves of the drilled shaft TP1

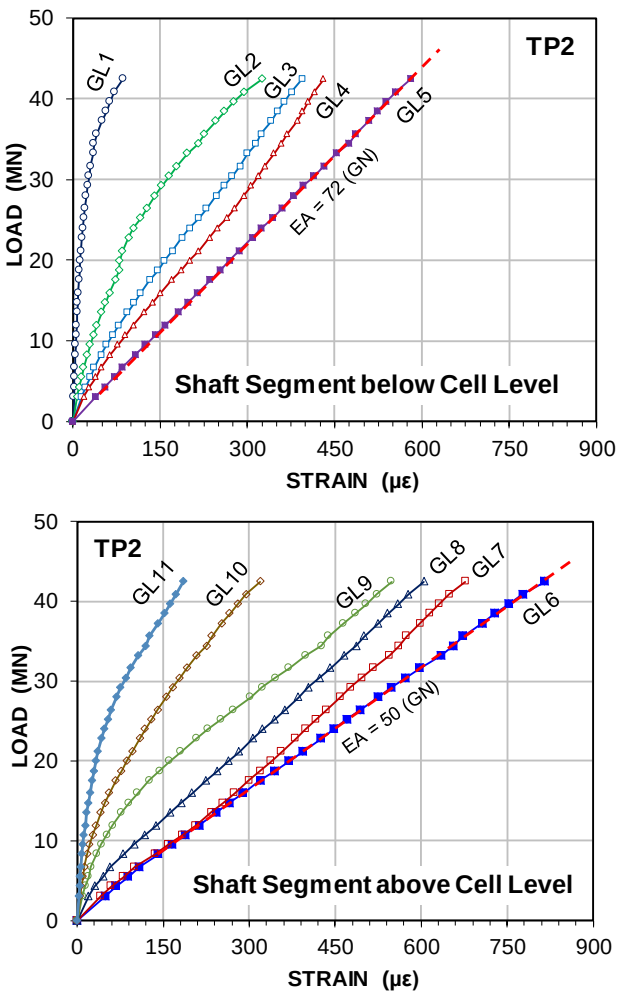

Figure 7 Load versus strain curves of the drilled shaft TP2

From the load-strain curves of the grouted shaft TP2 above the cell level (the lower diagrams of Figure 7), it is easy to recognize that the gage level GL6 is a good resource for evaluating the grouted shaft stiffness because the load-strain curve is relatively linear and the soil resistances from the cell level through this gage level (about 2.5 m) could be easily eliminated at the low load increment levels. It should be noted that this drilled shaft was grouted. The grouted shaft stiffness, EA, estimated from this gage level is about 50 GN.

As discussed earlier, theoretically adding this grout zone evenly to the shaft circumference and area means a 2.5% increase of circumference and a 5.0% increase of shaft cross section area. This means that the grouted shaft stiffness TP2 must be greater than the non-grouted shaft stiffness TP1. Therefore, and logically the strain measurements of the gage levels GL8 and GL9 in the non-grouted shaft TP1 are reasonable and reliable for the shaft resistance analysis.

The upper diagrams of Figure 7 display the load-strain curves of the grouted shaft TP2 below the cell level. The grouted shaft stiffness estimated from the gage level GL5 is about 72 GN, which is greater than the stiffness of the non-grouted shaft TP1 about 10 GN. The grouted shaft stiffness above the cell level is also greater than the non-grouted shaft of about 10 GN. If assuming that the concrete modulus of both tested shafts is equivalent, the cross-section areas of the grouted shaft below the cell level were increased about 16 and 24%, respectively. In addition, it has become clearly that the stiffness of the drilled shaft below and above the cell level are different dramatically. Therefore, it is more reasonable to separate the shaft segments below and above the cell level for the shaft shear analysis from the strain measurements.

4.4 Axial Tangent Stiffness of Drilled Shafts

Axial tangent stiffness (AE_t) of the drilled shafts is an important parameter for evaluating the shaft resistances measured from the installed strain gages. Normally, to convert the measured strain values to load, it is necessary to know the modulus of the drilled shaft material; however, the cross-section area of drilled shafts is variable significantly versus the drilled shaft depth. Therefore, the combination of shaft material modulus and cross-section area of shaft at the gage levels, which is known as axial stiffness of shaft (AEt), is important to evaluate the shaft shear resistances from the measured strain gage data. A small change of shaft stiffness will result in a significant change of the shaft shear resistance. In the above section, the stiffness of the drilled shafts was estimated from the slopes of the load-strain curves.

Fellenius (1989; 2018) recommended that the best way to evaluate the shaft material stiffness from the strain measurements is the tangent stiffness method because the load at a gage level is a function of the shaft material stiffness for the combination of the concrete and the steel reinforcement installed in the drilled shafts.

Figures 8 and 9 gives the stiffness-versus-strain plots of the non-grouted and grouted shafts TP1 and TP2, respectively. As the tangent stiffness showed to be independent of the strain level, the shaft stiffness values estimated from the tangent modulus method agree with those estimated from the load-strain slope method for the same gage levels. Therefore, to convert the measured strains into load, the constant stiffnesses, AE, of 62 through 72 GN and 42 through 52 GN will be used for the shaft segment below and above the cell level of the non-grouted and grouted shafts TP1 and TP2, respectively.

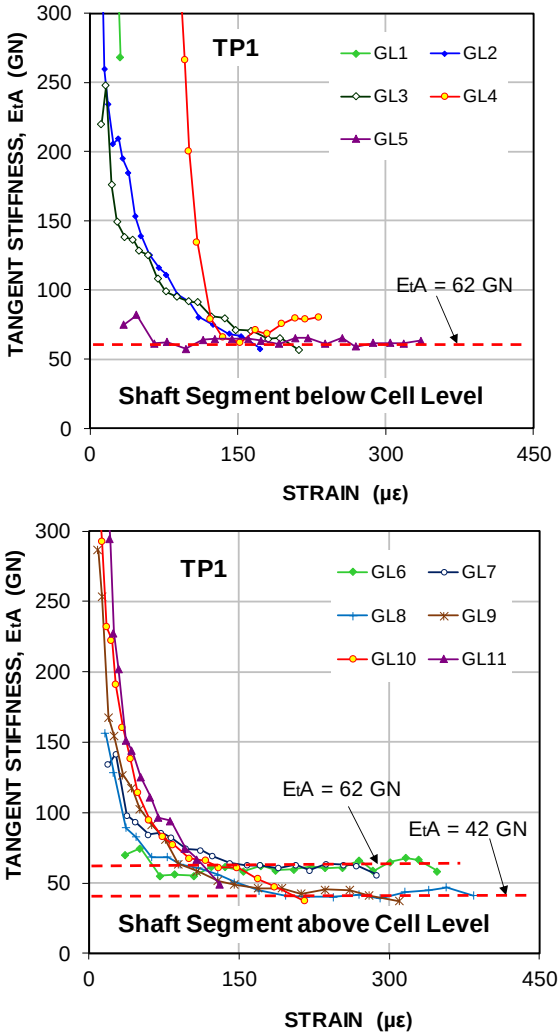

Figure 8 Stiffness Plots of the non-grouted shaft TP1

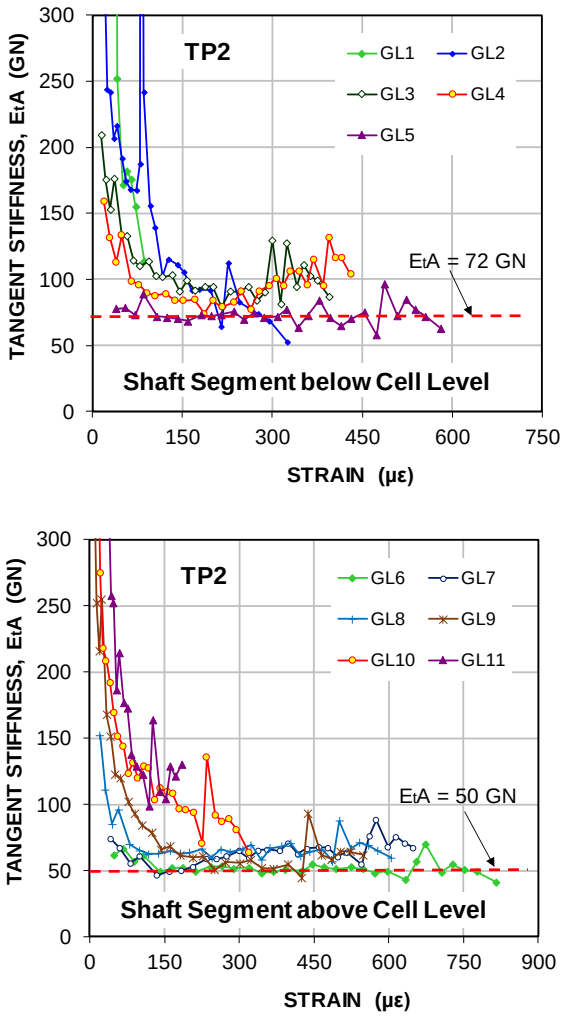

Figure 9 Stiffness Plots of the non-grouted shaft TP2

4.5 Shaft Stiffness from Elastic Shortening Measurements

The elastic shortenings had obtained from difference of the movements measured at the cell levels and at the top and bottom of the tested shafts. Figure 10 presents the elastic shortenings of shafts below and above the cell level versus the imposed test loads. The first striking observation from the diagrams is that the elastic shortening-load curves of the shafts below the cell levels are relatively linear; while, those above the cell levels are relatively non-linear and have more gentle slopes due to the influences of the different lengths and the mobilized soil shear resistances along the shaft lengths. From diagrams of the load-elastic shortening curves, it appears that the shaft resistances below the cell levels are significantly lower than those above the cell level and it is likely that this resulted from the difficulty of the shaft construction below the cell level due to presence of the cell equipment as mentioned earlier.

The next remarkable observation is that the compression of the shafts below the cell levels is greater that of those above the cell levels for the equivalent loading levels less than 13 and 26 MN for the shafts TP1 and TP2, respectively. It is noted that the shaft lengths below the cell levels are about 2.4 through 2.6 times shorter than those above the cell levels (Figure 3). Consider elastic shortening of 2.0 mm, the loads above the cell levels are about 3.0 and 4.0 MN greater than those below the cell levels for shafts TP1 and TP2 (including the shaft buoyant weights above cell levels of about 1.5 MN), respectively. If subtracting the shaft buoyant weights above cell levels of about 1.5 MN, these differences are about 1.5 and 2.5 MN, respectively. These also imply that the shaft resistances below the cell levels are significantly lower than those above the cell levels.

To confirm the shaft stiffnesses estimated from the strain gage measurements, it is necessary to employ the theoretical elastic compression equation (1) to calculate the shaft stiffnesses from the measured elastic shortenings as follows:

$$S_e = \frac{QL}{AE} \tag{1}$$

where,

S_e = Elastic shortening;
Q = Applied load;
L = Length of shaft;
AE = Stiffness of shaft.

The elastic compression in this case refers to the shaft deflection that would occur if 100 percent of the applied load was transferred to the toe and head of the shaft (i.e., zero shaft friction). The results of elastic compression are given in Table 1.

Logically, if absence of the positive residual loads in the drilled shafts before testing, the measured elastic shortenings must be smaller than the theoretical calculated elastic compression from equation (1) due to presence of the soil shear resistances along the constructed shafts. The calculated results presented in the above table show that the calculated elastic shortenings for the stiffnesses estimated from the strain gage measurements are less than the measured elastic shortenings. Therefore, the shaft stiffnesses estimated from the above strain gage measurements are reasonable for the drilled shaft resistance analysis.

Table 1 Back-calculation of Elastic Shortenings from the Estimated Shaft Stiffnesses

Shaft	Max. Test Load (MN)	Shaft Length (m)		Shaft Stiffness, AE (MN)		Elastic Shortening of Shaft below Cell Level (mm)		Elastic Shortening of Shaft above Cell Level (mm)	
		Below Cell Level	Above Cell Level	Below Cell Level	Above Cell Level	Calculated	Measured	Calculated	Measured
TP1	21.64	25.0	60.0	62,000	42,000	8.73	7.16	30.91	9.63
TP2	42.46	23.5	61.5	72,000	50,000	13.86	11.68	52.23	14.73

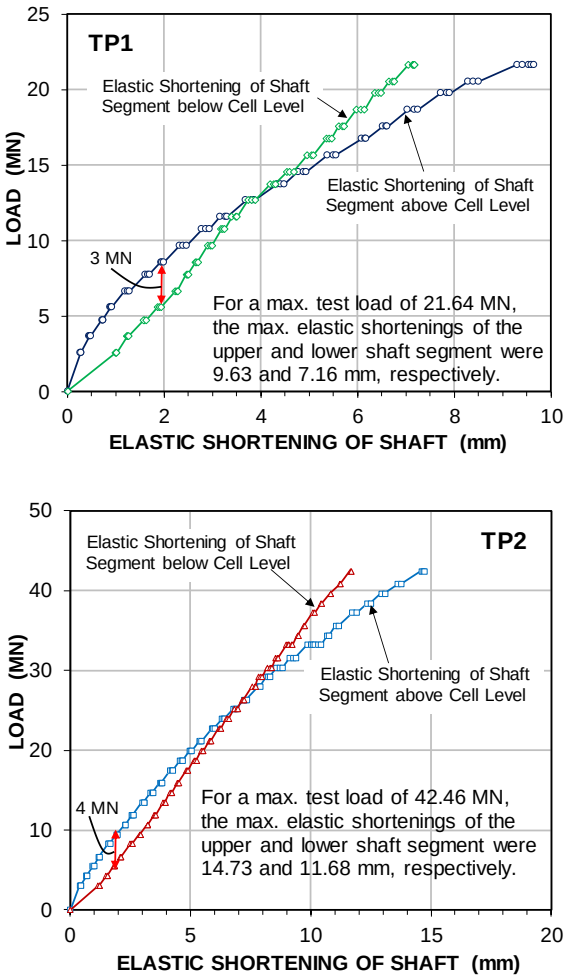

Figure 10 Plots of the elastic shaft shortening versus test load

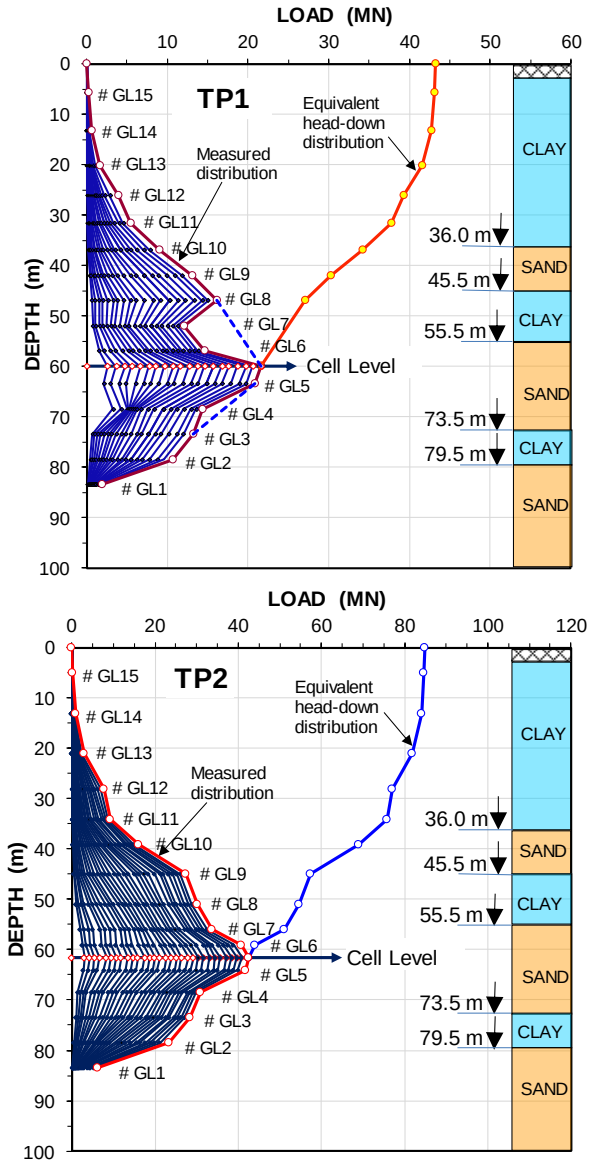

Figure 11 Load Distributions and Equivalent Top-down Curves of the Shafts TP1 and TP2

4.6 Load Distributions

The shaft stiffnesses of 62 through 72 GN and 42 through 50 GN below and above the cell levels were used to convert the average of strain measured at each gage level for each applied load. The results for the two tested shafts are shown in Figure 11. The lines of loads plotted above the cell level connect to the respective cell loads and the lines below connect to a respective cell loads. Figure 11 also show the equivalent head-down load-distribution curves of two tested shafts. It is noted that the buoyant pile weights above the cell levels were not subtracted and the residual loads were not included. The water pressures at the cell levels were not measured and were not considered.

The upper diagrams of Figure 11 show the load distributions of the non-grouted shaft TP1. It is easy to recognize that load distributions from the cell level through the gage level GL7 are not reasonable. Hence, the load distributions above the cell levels will becomes more reasonable if connecting the cell level with the gage level GL8. In addition, for the gage GL4 below the cell level, the initial load distributions are not also reasonable. As discussed earlier, the strain records of this gage level are not reliable as can be seen from the upper diagrams in Figure 5 and thus connecting the gage level GL3 with GL 5 (the upper diagrams of Figure 11) shows the more practical load distributions. The lower diagrams of Figure 11 show the load distributions of the grouted shaft TP2. In general, the

load distributions obtained from the strain gage measurements are relatively reasonable.

As can be observed from the load distribution curves, the toe resistances were not mobilized significantly.

4.7 Shaft Shear Resistance versus Movements

Figures 12 and 13 provides the average unit shaft shear resistances versus movements of the non-grouted and grouted shafts TP1 and TP2, respectively. The average unit shaft shear resistance between the gage levels were determined as the difference in evaluated strain-gage load divided by the surface area between the gage levels. The gage levels below and above the cell levels are plotted against the downward and upward movements, respectively.

For the unit shear resistances of shaft TP1 in Figure 12, the records of strain gages at the gage level, GL4, GL6 and GL7 were considered unreliable and are therefore omitted. In this case, the unit shear resistances were calculated from GL3 through GL5 and from the cell level through GL8. As can be seen from the upper diagrams of Figure 12, the unit shear resistances of the sand layers below the cell level differ significantly from each other.

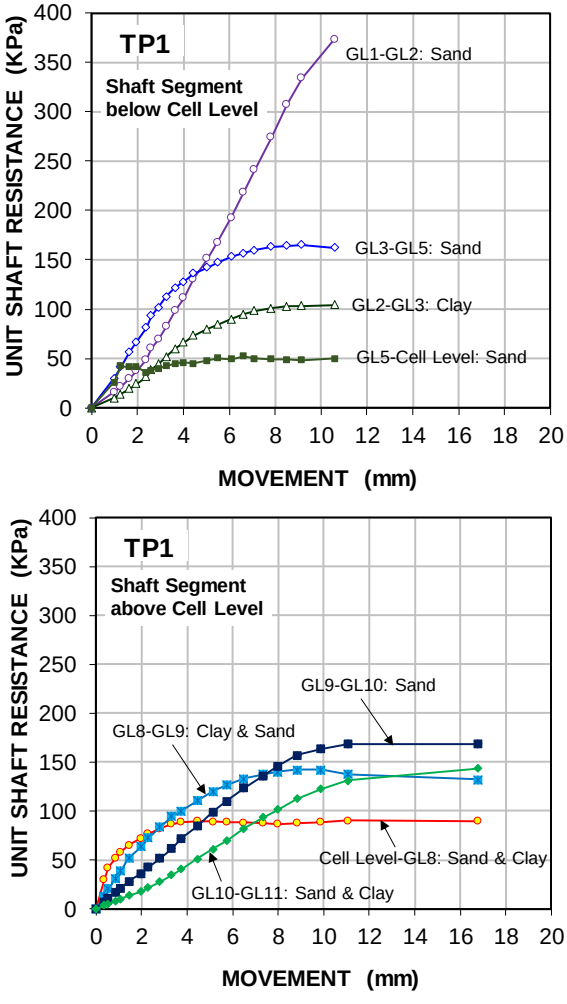

Figure 12 Unit Shaft Resistances versus Movements of the Non-Grouted Shaft TP1

The unit shaft resistance of sand layer from the cell level through GL5 is about 50 kPa, which is a half of that of the clay layer from GL2 through GL3. In addition, the unit shaft resistances of sand layer from the GL3 through GL5 and GL9 through GL10 is relatively low, only about 165 kPa. It is clear that the unit shaft resistances of sand layer from the cell level through GL3 did not reflect the actual soil conditions at these depths. It is noted that the shear strengths of the sand layers along the tested shafts are relatively equivalent as shown on the SPT N-Indices diagram in Figure 2. Therefore, it seems that the shear resistances for shaft TP1 at these depths were affected by the presence of left-behind slurry filter cake between the shaft and the soil. In the strain gage measurements of the shaft TP1, the unit shaft resistance of GL1 through GL2 is relatively reasonable for the shear resistance of the sand layer. However, the GL1-GL2 unit shear resistance curve does not show an ultimate value (strain-hardening) and thus the maximum measured unit shear resistance of about 370 kPa is representative for the shear resistance of sand layer. For the clay layer below the cell level, the unit shear resistance is about 100 kPa. The shaft segments from the cell level through GL9 and GL10 through GL11 that included both sand and clay layer and the unit shaft resistances ranged from 90 through 140 kPa.

Figure 13 shows the unit shear resistances of the grouted shaft TP2. Similar to the non-grouted shaft TP1, the unit shear resistances of the sand layers below the cell level are significantly different. The unit shaft resistances of sand layer from the cell level through GL5 and GL3 through GL4 (the upper diagrams of Figure 13) are very low, only about 50 and 150 kPa, respectively, which are equal to the unit shear resistances of Shaft TP1 at the similar depths.

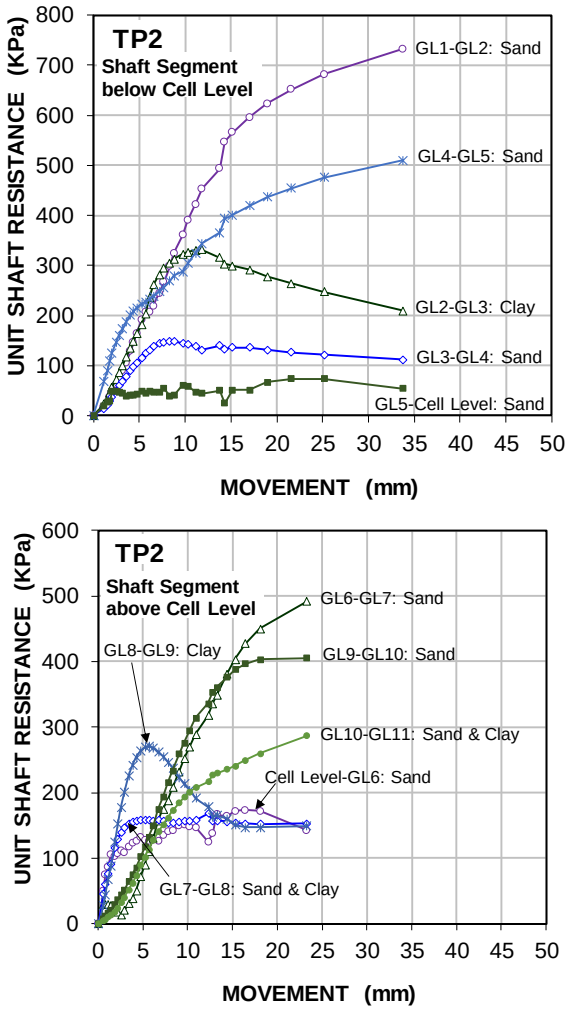

Figure 13 Unit Shaft Resistances versus Movements of the Non-Grouted Shaft TP2

The cell-GL6 shear resistance of sand layer (the lower diagram of Figure 13) measured is only about 150 kPa. It is no doubt that these unit shaft resistances did not reflect the actual soil conditions at these depths. It is likely that the shear resistances at these depths were also affected by the presence of left-behind slurry filter cake between the shaft and the soil as shaft TP1. Only the unit shaft resistances of GL1-

GL2, GL4-GL5, GL6-GL7 and GL9-GL10 ranging from 400 to 730 kPa are relatively reasonable for the grouted shafts placed in the dense sand layer. The average unit shaft resistance of these gage levels is about 535 kPa, which is about 1.45 times greater than that of the non-grouted shaft TP1 in dense sand layers. For the grouted shaft in the clay layers, the average unit peak shear resistance of GL2-GL3 and GL8-GL9 is about 300 kPa, which is about 3.0 times greater than that of the non-grouted shaft TP1. In the subject case, the effectiveness of the grouted shaft in clay layer is about 2.0 times greater than in sand layer. In addition, the movements necessary to mobilize fully most of the ultimate shaft resistances ranged from 5 to 15 mm.

4.8 Effectiveness of Post-Grouting Shaft

The effectiveness of the grouted shaft obtained preliminarily from the load-movement curves is about 1.5. The effectiveness of the grouted shaft estimated from the strain gage measurements is about 1.45 and 3.0 for sand and clay layers, respectively. To validate the effectiveness of the shaft grouting obtained from the load-movement measurements and the strain gage analysis, the unit shear resistance of shafts below the cell level will be determined from the test load divided by the surface areas of shafts below the cell levels (including the toe areas).

The upper diagrams in Figure 14 shows the unit shear resistance-movement curves of the non-grouted and grouted shafts TP1 and TP2, respectively. To evaluate the effectiveness of the shaft grouting, the unit shear resistances of the shaft TP1 was extrapolated using hyperbolic function as can be seen from the green dash curves in the upper diagrams of Figure 14. The lower diagram of Figure 14 presents the effectiveness of the shaft grouting versus movements.

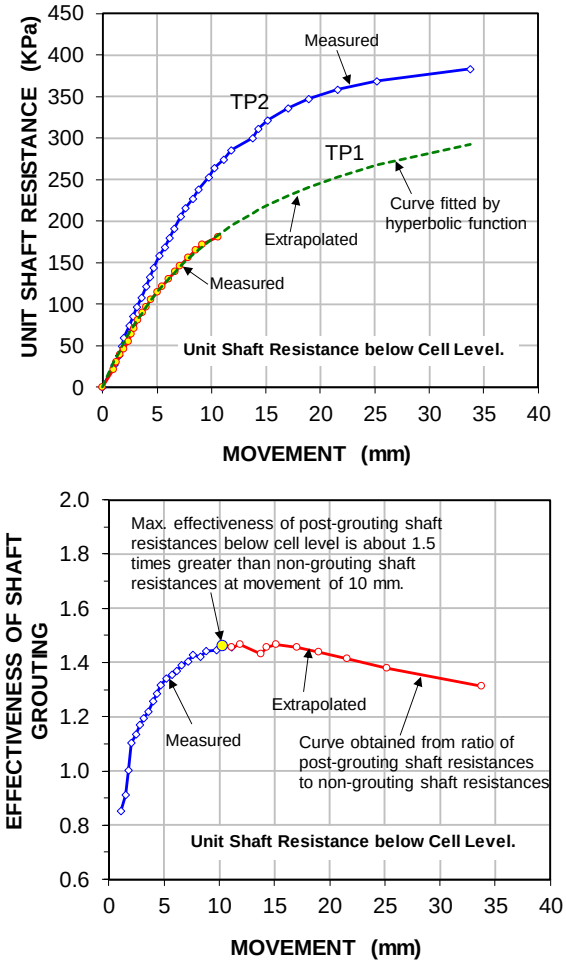

Figure 14 Unit Shaft Resistances versus Movements below the Cell Levels and Effectiveness of the Shaft Grouting

The maximum effectiveness of the shaft grouting based on the measured data is about 1.47 for the shaft resistances below the cell levels, which is approximate with the shaft grouting effectiveness determined from the load-movement measurements and the strain gage analysis of sand layer.

5. CONCLUSION

The two bidirectional-cell tests on the non-grouted and grouted shafts were reported. The analysis of the load-movements curves and the strain gage measurements were also performed and presented. The following conclusions can be drawn from the present study.

The unit shaft resistances of the sand and clay layers were increased about 150 and 300 percent after grouting, respectively. The average unit shaft resistance of the 49-m grouted shaft is about 1.5 times greater than that of the non-grouted shaft.

The shaft and toe resistances for both tested shafts were affected by presence of slurry filter cake between the concrete and the soil.

The strain gage levels installed close to the cell level are useful for evaluating the shaft stiffnesses, but not reliable for evaluating the shaft shear resistances.

The shaft stiffness below and above the cell level of the bidirectional loading tests should be separated for evaluating the shaft resistances measured from strain gages.

The elastic shortening parameter of the tested shafts is useful for validating the shaft stiffness values estimated from the strain gage measurements.

The unit shaft shear resistances obtained from the test loads divided by the surface areas of shafts below the cell levels (including the toe areas) are useful for validating the unit shaft resistances estimated from the strain gage measurements.

6. REFERENCES

Bolognesi, A.J.L., and Moretto, O., 1973.Stage grouting preloading of large piles on sand. Proc., 8th ICSMFE, August 12-19, Moscow, Vol. 2.1, pp. 19-25.

Bruce, D. A. 1986. Enhancing the performance of large diameter piles by grouting, Parts 1 and 2, Ground Engng., 19(4) 7 and 19(5) 7.

Fellenius, B.H., 1989. Tangent modulus of piles determined from strain data. ASCE, Geotechnical Engineering Division, the 1989 Foundation Congress, F.H. Kulhawy, Editor, Vol. 1, pp. 500-510.

Fellenius, B.H., 2001. From strain measurements to load in an instrumented pile. Geotechnical News, Vol. 19, No. 1, pp 35 - 38.

Fellenius, B.H., 2002. Determining the true distribution of load in piles. Proceedings of International Deep Foundation Congress, An international Perspective on Theory, Design, Construction, and Performance, American Society of Civil Engineers, ASCE, GSP 116, O'Neill, M.W. and Townsend, F.C., Editors, Orlando, Florida, February 14 - 16, 2002, Vol. 2, pp. 1455 - 1470.

Fellenius BH (2018) Basics of foundation design—a textbook. Pile Buck International, Inc., Vero Beach. Electronic Edition, www.Fellenius.net.

Loadtest International Pte. Ltd., 2016. Reports on Bored Pile Testing, Lancaster Lincoln, Vietnam, 168281-DR01-00 and 168281-DR02-00, 82 p and 89 p.

Nguyen, H.M., Fellenius, B.H., Puppala, A.J. Aravind, P., and Tran, Q.T.2016. Bidirectional Tests on Two Shaft-Grouted Barrette Piles in the Mekong Delta, Vietnam. Geotechnical Engineering Journal of the SEAGS & AGSSEA 47(1) 15-25.